Supplementary Figures

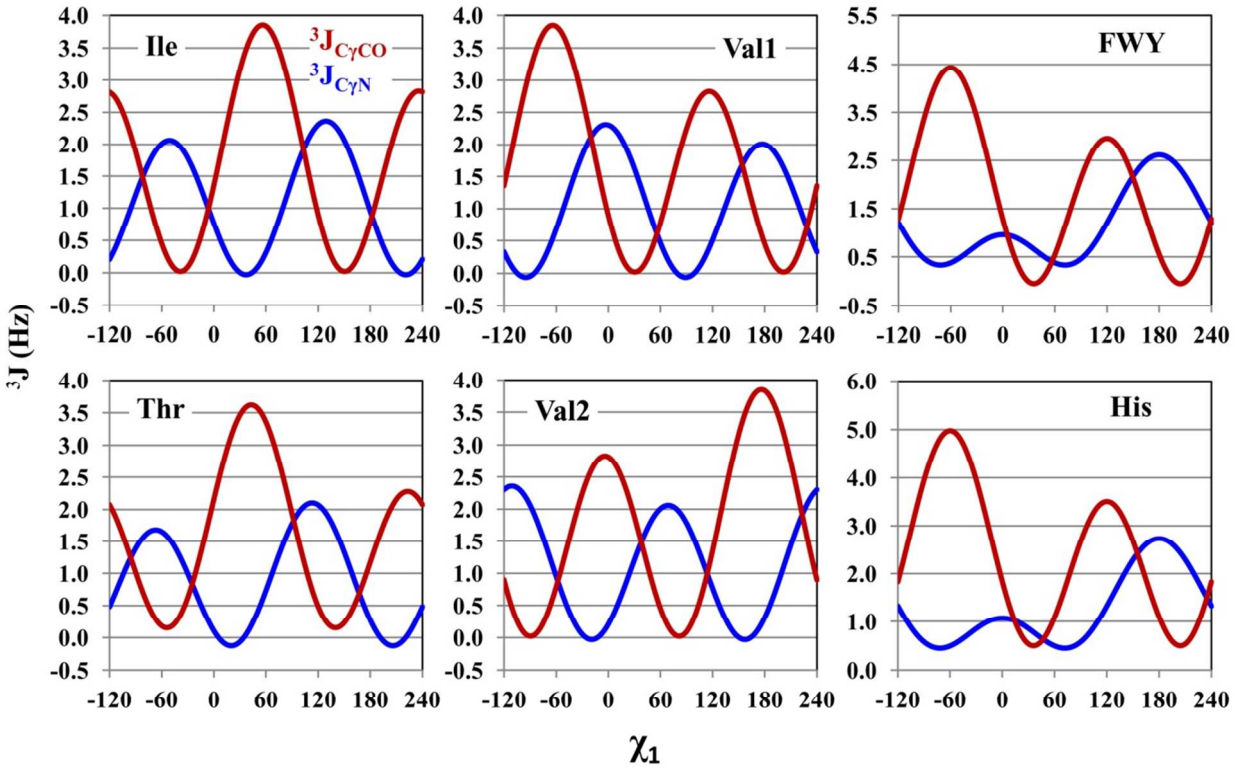

Figure S1. Karplus curves for $^3J_{C\gamma N}$ (blue) and $^3J_{C\gamma CO}$ (red) used to determine the staggered rotamer populations according to Equations 1-3 in the main text. Parameters for Ile, Thr, and Val are from Chou et al.,[1] parameters for FWY and His are from Tuttle et al.[2]

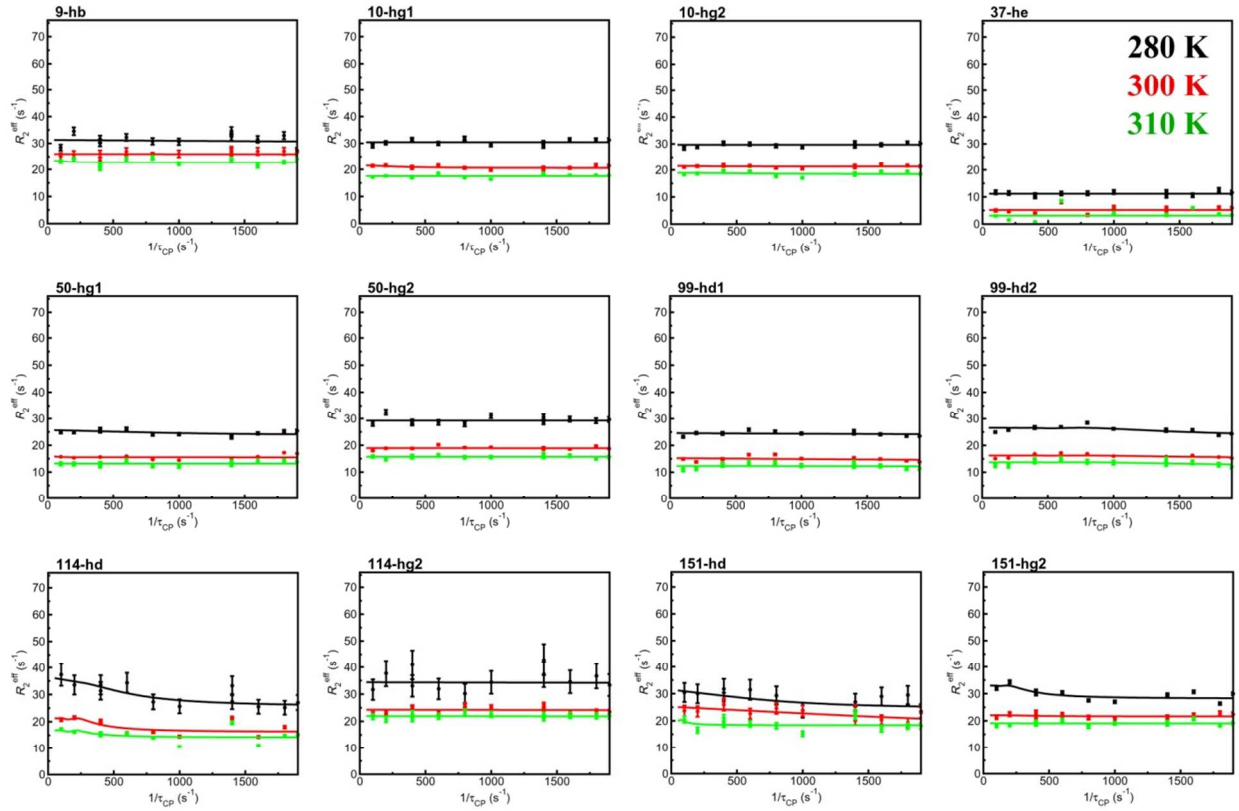

Figure S2. Representative $^{13}C_{methyl}$ R_2 relaxation dispersion curves for hE:FOL:NADP+ at 280 K (black), 300 K (red), and 310 K (green). Experiments were performed at 800MHz. Ile114-Cδ and Ile151-Cγ2 show hints of dispersion at 280K, but clear $^{13}C_{methyl}$ dispersion is not observed for other methyl-containing residues.

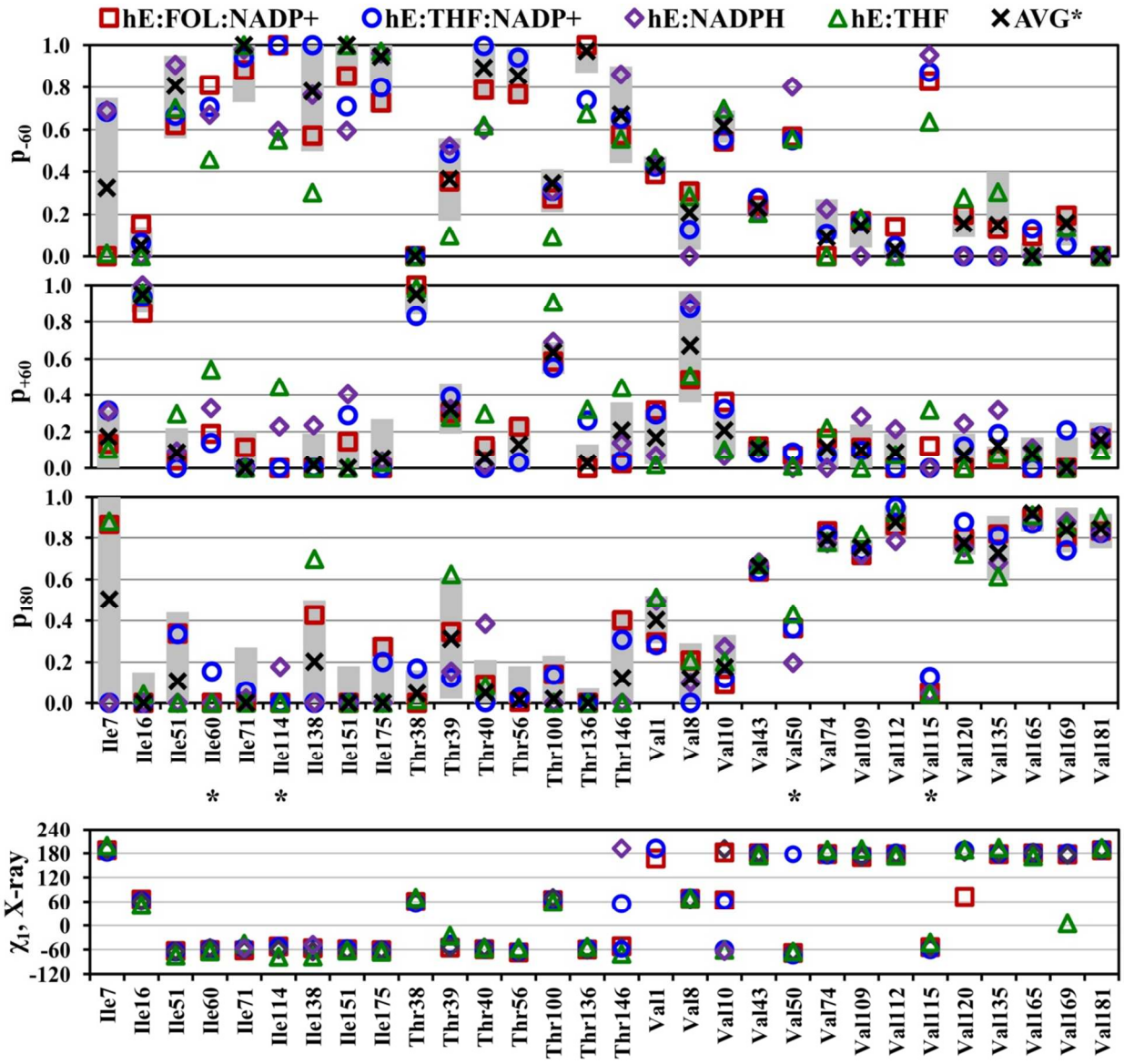

Figure S3. Staggered rotamer populations for Ile, Thr, and Val residues (top panels). Populations fit to the hDHFR all-complex average is shown as an X. Complexes are excluded if the error in the coupling is larger than 1Hz. Errors (shaded bars) are shown for the AVG fit based on the population ranges determined from ${}^3J_{avg} \pm \sigma$. Asterisks indicate residues with unique rotamer averaging in one or more complex. Bottom panel: χ_1 dihedral angle from the hDHFR X-ray structures: hE:FOL:NADP$^+$ (4M6K), hE:THF:NADP$^+$ (4M6L), and hE:NADPH (4M6J) coordinates are from Bhabha et al,[3] hE:THF is from 1DHF.[4]

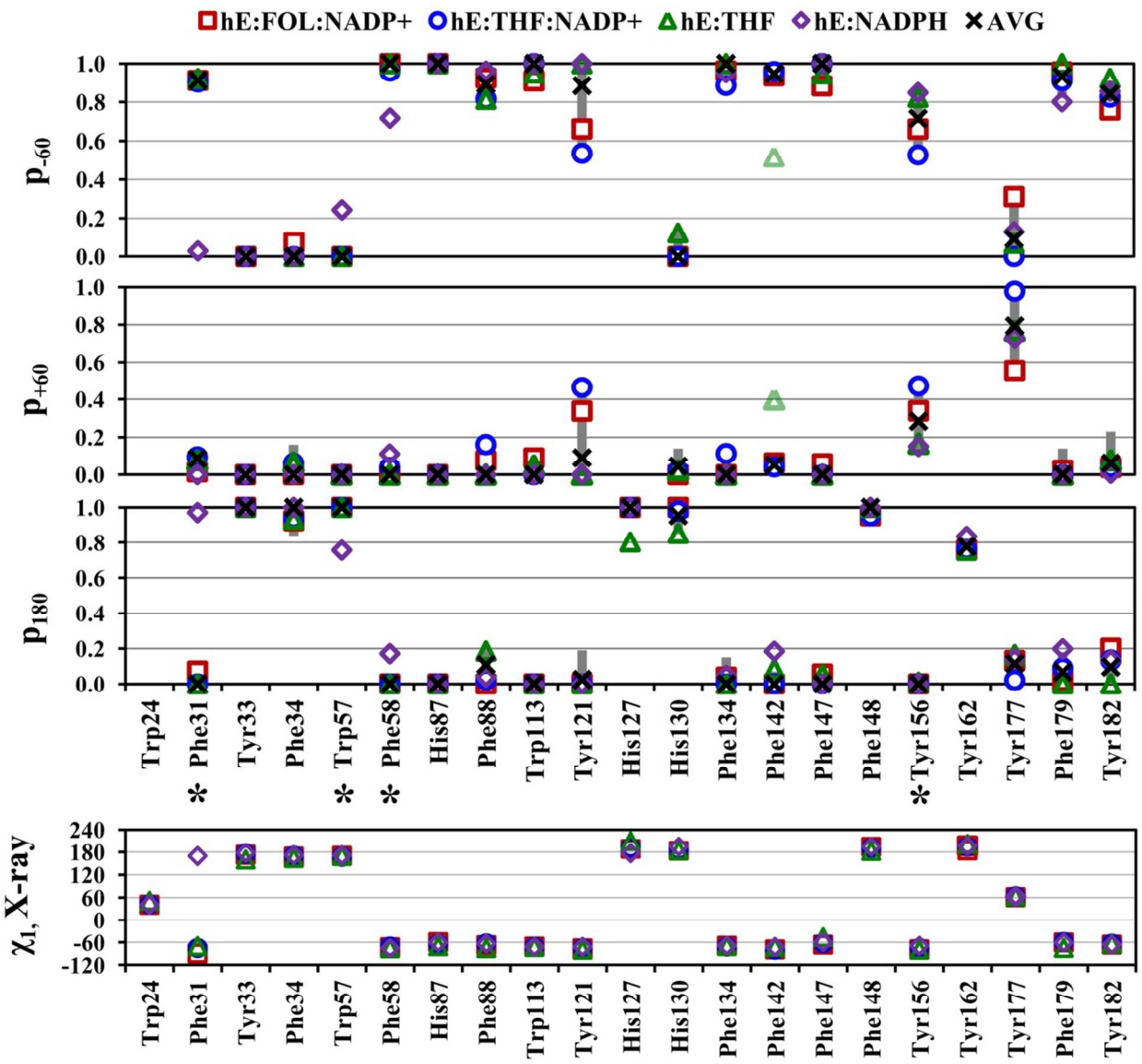

Figure S4. Staggered rotamer populations for aromatic residues (top panels). Populations fit to the hDHFR all-complex average is shown as an X. Complexes are excluded from this average if the error in the coupling is larger than 1Hz. Errors (shaded bars) are shown for the AVG fit based on the population ranges determined from $^{3}J_{avg} \pm \sigma$. Asterisks indicate residues with unique rotamer averaging in one or more complex. hE:THF Phe142 p_{-60} is a lower bound. Bottom panel: χ_1 dihedral angle from the hDHFR X-ray structures: hE:FOL:NADP$^+$ (4M6K), hE:THF:NADP$^+$ (4M6L), and hE:NADPH (4M6J) coordinates are from Bhabha et al,[3] hE:THF is from 1DHF.[4]

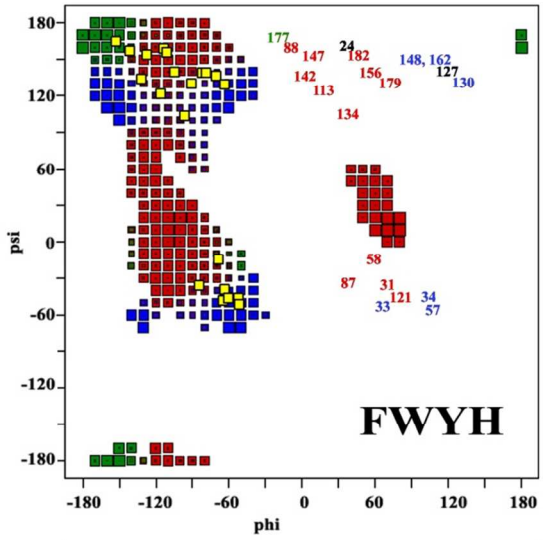
FWYH
psi
phi

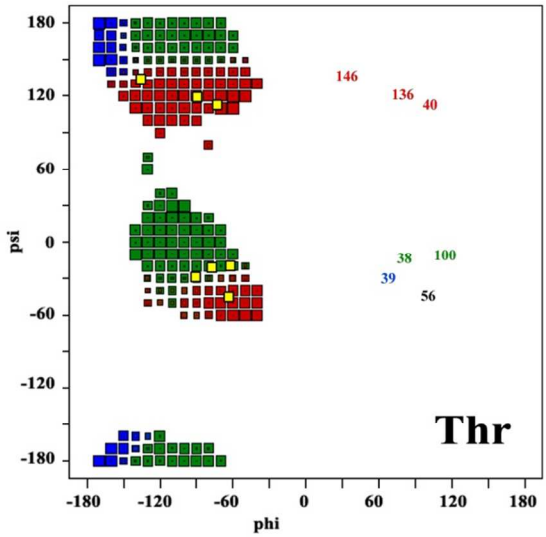
Thr
psi
phi

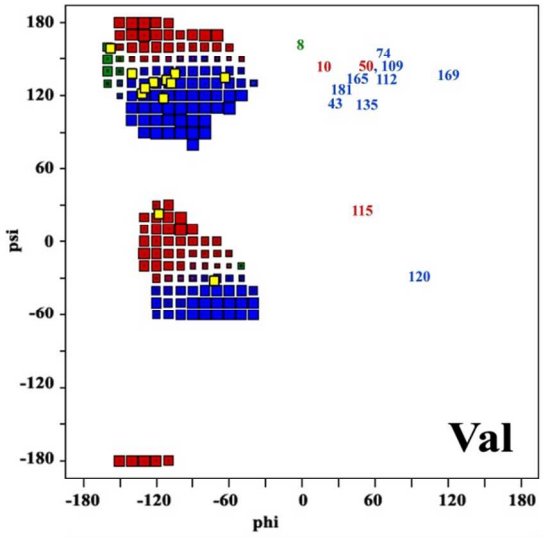
Val
psi
phi

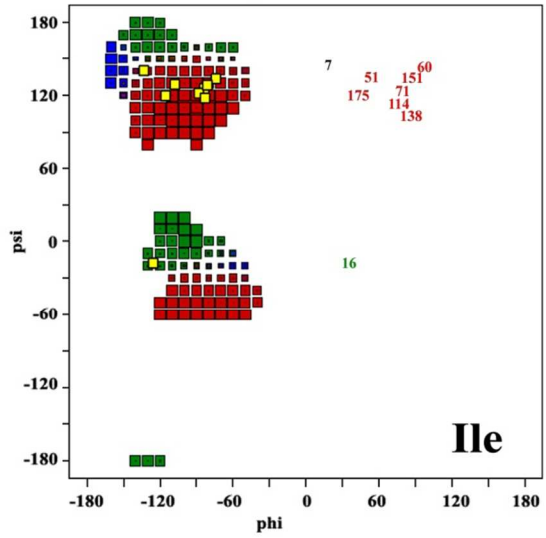
Ile
psi
phi

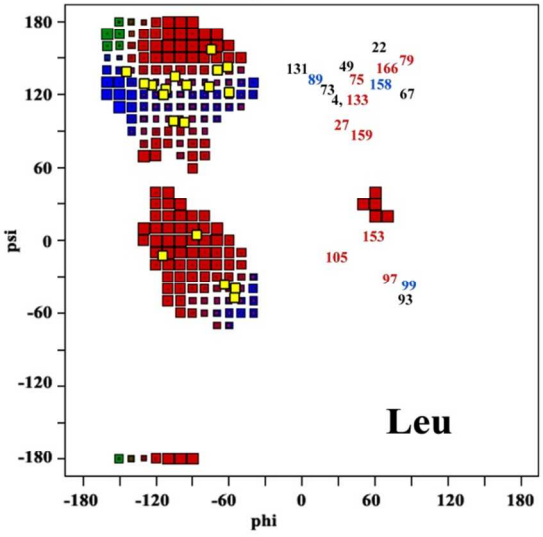
Leu
psi
phi

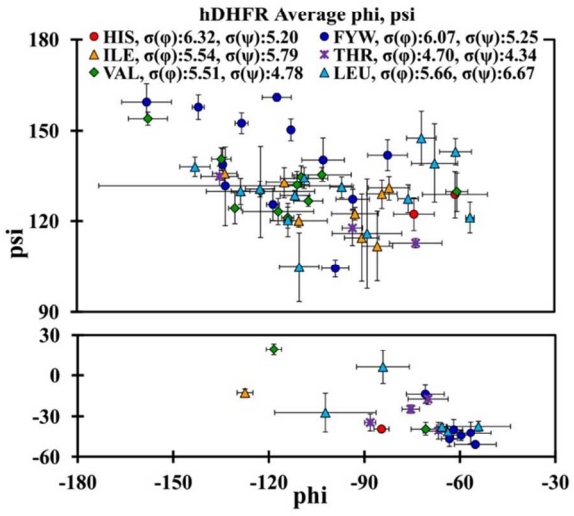
hDHFR Average phi, psi
HIS, σ(φ):6.32, σ(ψ):5.20
FYW, σ(φ):6.07, σ(ψ):5.25
ILE, σ(φ):5.54, σ(ψ):5.79
THR, σ(φ):4.70, σ(ψ):4.34
VAL, σ(φ):5.51, σ(ψ):4.78
LEU, σ(φ):5.66, σ(ψ):6.67
psi
phi

Figure S5. Ramachandran box plots based on the Dunbrack backbone dependent rotamer conformations.[5] Panels for aromatics, Thr, Val, Ile, and Leu: red (χ_1=-60^o), blue (χ_1=180^o), and green (χ_1=+60^o) squares show the propensity of each staggered χ_1 rotamer to be sampled based on the backbone ϕ, ψ dihedral; the size of the square is related to the probability of that rotamer. Yellow squares show the ϕ, ψ values from the hDHFR:FOL:NADP$^+$ X-ray structure[3] with residue labels offset to the right, colored according to the ^{3}J-based major rotamer (or in black if not determined due to large errors and/or resonance overlap). Bottom right panel: The average ϕ, ψ values for the complexes of hDHFR (hE:FOL:NADP$^+$, 4M6K; hE:THF:NADP$^+$, 4M6L; hE:NADPH, 4M6J; and hE:THF as modeled by hE:FOL, 1DHF); error bars show the standard deviation in the ϕ and ψ angles.

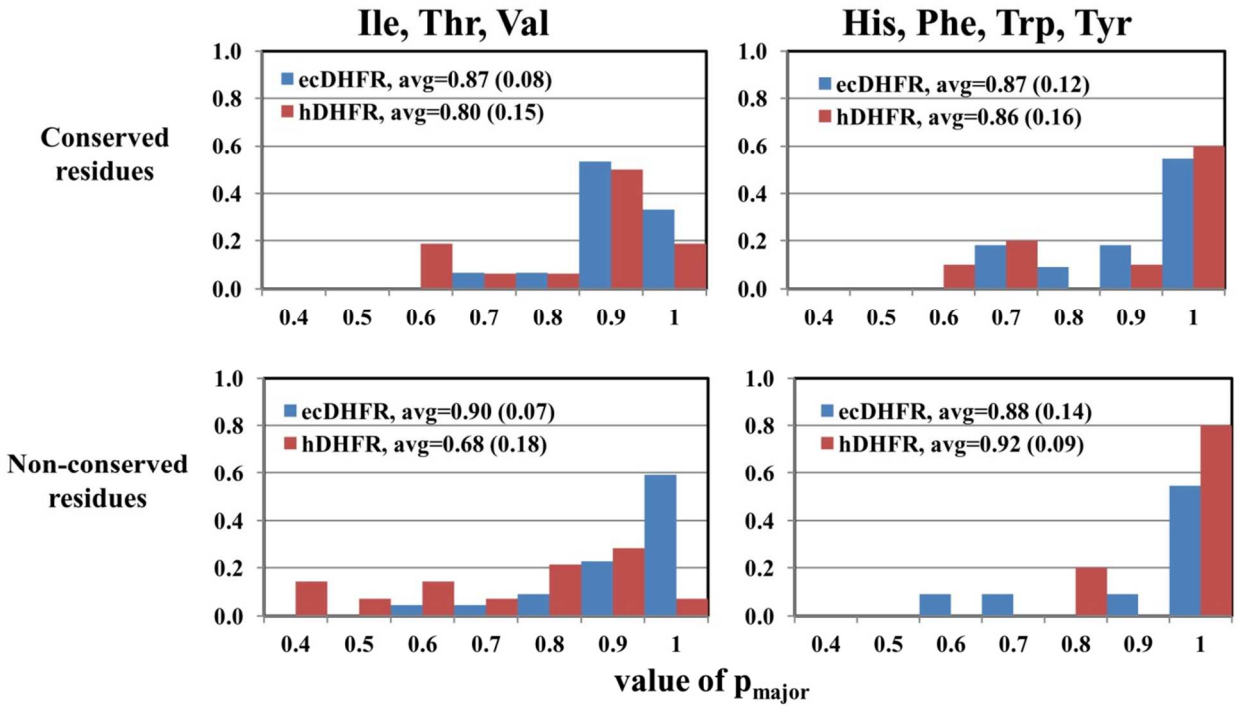

Figure S6. Distribution of p_{major} in hDHFR and ecDHFR E:FOL:$NADP^+$. Top row shows the distribution for the identical and conserved residues (green and cyan residues in Figure 8A). Bottom rows show the distribution for the methyl and aromatic residues in hDHFR and ecDHFR that do not have equivalent residues in the other species. The conserved residues have remarkably similar distributions of p_{major} whereas for the non-conserved residues, hDHFR shows more rotamer averaging for the methyl residues and less rotamer averaging for its unique aromatic residues.

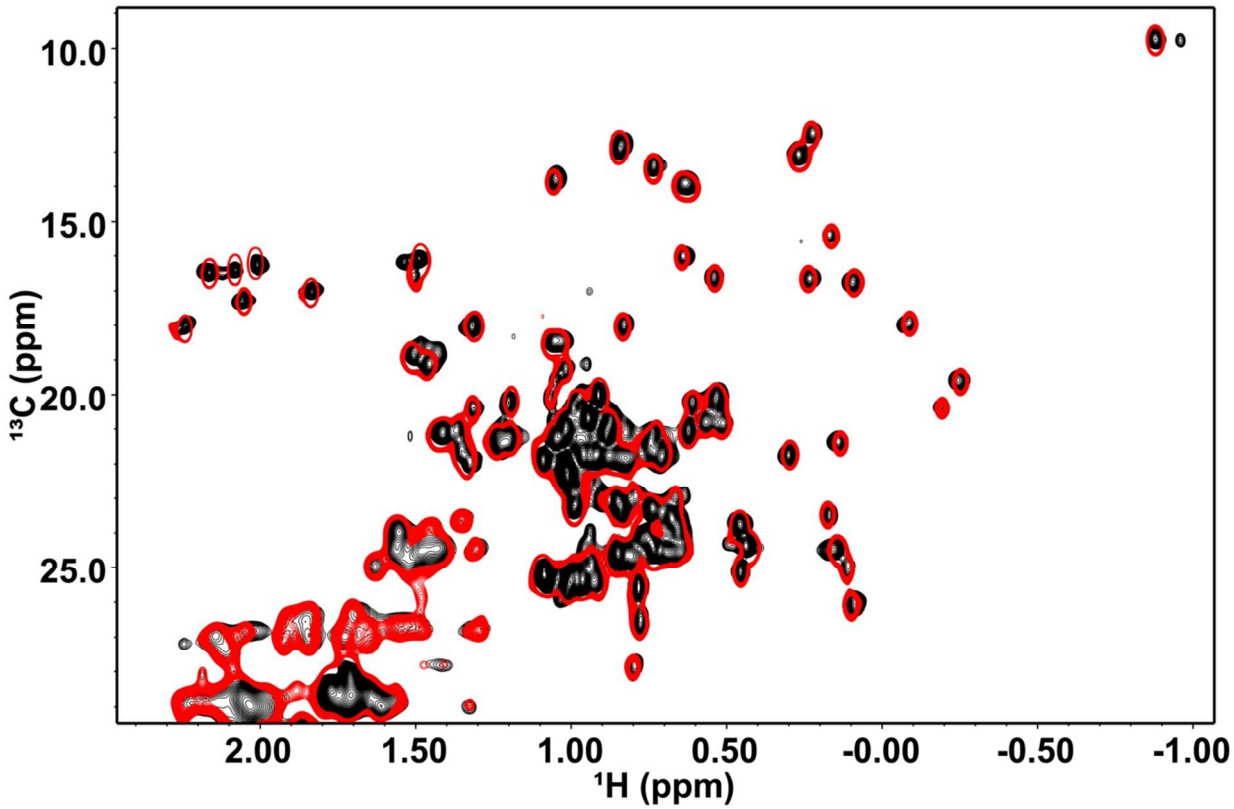

Figure S7. Overlay of the ^{13}C-HSQC methyl region of hE:THF:NADP^{+} (black) and hE:FOL:NADP^{+} (red). The near identity of the spectra indicate that bound THF and FOL interact in a very similar manner with the protein backbone and side chains in the ternary complexes.

References

1. Chou, J. J., Case, D. A., and Bax, A. (2003) Insights into the Mobility of Methyl-Bearing Side Chains in Proteins from 3JCC and 3JCN Couplings, *Journal of the American Chemical Society 125*, 8959-8966.
2. Tuttle, L. M., Dyson, H. J., and Wright, P. E. (2013) Side-Chain Conformational Heterogeneity of Intermediates in the Escherichia coli Dihydrofolate Reductase Catalytic Cycle, *Biochemistry 52*, 3464–3477.
3. Bhabha, G., Ekiert, D. C., Jennewein, M., Zmasek, C. M., Tuttle, L. M., Kroon, G., Dyson, H. J., Godzik, A., Wilson, I. A., and Wright, P. E. (2013) Divergent evolution of protein conformational dynamics in dihydrofolate reductase, *Nat Struct Mol Biol*.
4. Davies, J. F., 2nd, Delcamp, T. J., Prendergast, N. J., Ashford, V. A., Freisheim, J. H., and Kraut, J. (1990) Crystal structures of recombinant human dihydrofolate reductase complexed with folate and 5-deazafolate, *Biochemistry 29*, 9467-9479.
5. Shapovalov, M. V., and Dunbrack, R. L. (2011) A Smoothed Backbone-Dependent Rotamer Library for Proteins Derived from Adaptive Kernel Density Estimates and Regressions, *Structure 19*, 844-858.